

RESEARCH

Open Access



The color influence of dust in air pollutants on architectural painting: a case of archery tower at the West Gate in Shaanxi, China

Juanli Wang¹, Ming Cao², Peng Fu³ and Wenqiang Dong^{1*}

Abstract

At present, under the influence of environmental pollution, the color of architectural painting gradually darkens, loses luster, and even cracks when the pigment falls off, which seriously affects the long-term preservation of architectural painting. In order to study the damage mechanism of dust particles to the color of the architectural painting, this study took the archery tower at the West Gate as the research object, monitored the temperature and humidity of the indoor environment, and analyzed the composition of the dust by ICP-MS, IC, and XRD. The experimental results showed notable fluctuations in the indoor humidity in inner the archery tower at the West Gate during the monitoring period from January to March, which were not conducive to the preservation of wood-colored paintings. The 24-h average PM_{2.5} and PM₁₀ concentrations, measured over 2 days in January, were beyond the National Ambient Air Quality Standard norms, and PM contains a large amount of soluble salts such as sulfate and nitrate, causing serious salt erosion and damage to the color painting layer. Through the simulation experiment of the color painting layer, it was revealed that the dust particles deposited on the surface of the color painting layer change the spectral characteristics of the color painting layer, and then cause the color layer to lose its original hue, fade become blurred, or darken. It was anticipated that this research would serve as a valuable reference for the preventive protection of the color painting layer of the archery tower at West Gate.

Keywords Air pollutants, Architectural painting, Dust, Archery tower

Introduction

The city wall is the main mark of human beings entering a civilized society. With the development of history, the city wall system and auxiliary structures have become more sophisticated to meet evolving defense needs.

During the Ming and Qing Dynasties, the construction of the city wall reached a mature stage in China. The city wall of Xi'an in the Ming Dynasty is the most typical city wall building in this period.

The ancient city gate was the entrance and exit of the city, and it was the main target for both the offensive and defensive in wartime. With the continuous development of offensive and defensive tactics, the establishment of the city gate also unceasingly strengthened the defensive function. There were four gates in Xi'an City in the Ming Dynasty, namely South Yongning Gate, North Anyuan Gate, East Changle Gate, and West Anding Gate. The construction system of the four city gates is basically the framework of three-layer walls and three-story towers. The three-story towers are the brake tower, the arrow tower, and the main tower. Since the 4th year of

*Correspondence:

Wenqiang Dong
dongwq@nwpu.edu.cn

¹ Key Laboratory of Archaeological Exploration and Cultural Heritage Conservation Technology, Ministry of Education, Institute of Culture and Heritage, Northwestern Polytechnical University, Xi'an 710072, Shaanxi, China

² Cultural Property Protection Center, Ningbo University of Finance & Economics, Ningbo 315175, China

³ Shaanxi Institute for the Preservation of Cultural Heritage, Xi'an 710004, China



© The Author(s) 2024. **Open Access** This article is licensed under a Creative Commons Attribution 4.0 International License, which permits use, sharing, adaptation, distribution and reproduction in any medium or format, as long as you give appropriate credit to the original author(s) and the source, provide a link to the Creative Commons licence, and indicate if changes were made. The images or other third party material in this article are included in the article's Creative Commons licence, unless indicated otherwise in a credit line to the material. If material is not included in the article's Creative Commons licence and your intended use is not permitted by statutory regulation or exceeds the permitted use, you will need to obtain permission directly from the copyright holder. To view a copy of this licence, visit <http://creativecommons.org/licenses/by/4.0/>. The Creative Commons Public Domain Dedication waiver (<http://creativecommons.org/publicdomain/zero/1.0/>) applies to the data made available in this article, unless otherwise stated in a credit line to the data.

Hongwu in the Ming Dynasty, the arrow tower of the Yongning Gate, the main towers of Changle Gate and Anyuan Gate have been destroyed by war or collapsed. The main tower and arrow tower of Changle Gate were burned down in 1643 when Li Zicheng captured Xi'an in the late Ming Dynasty and were restored in the 13th year of Shunzhi in the Qing Dynasty (1656 AD). They had been restored to the style of the Changle Gate before it was burned down. The brake towers of the four gates in the Ming Dynasty no longer exist. The only city gate that preserves the archery tower (Fig. 1A, B) and the main tower of the Ming Dynasty is the Anding Gate (known as the West Gate). Through a survey, we discovered colored paintings of whirling-flower type on the beam, column, tiebeam, and purlin (Fig. 2b). The colors, including green, blue, black, white, yellow, and red, are elegant. The outer eaves are left with colorful paintings of the flame pearl pattern (see Fig. 1C) [1, 2]. The color paintings on the outer eaves of the archery tower at West Gate also have a distinctive feature. On the wooden components at the four corners of the outer eaves, there are also color paintings painted in the early Qing Dynasty, in the early days of the founding of the People's Republic of China, and in recent years (Fig. 1D). The artworks from different periods complement each other and are full of history. The colorful paintings on the inner eaves of the archery tower at West Gate contain rich historical information, which has important research value.

Unfortunately, due to the constant exposure to the natural environment, the continuous influence

of atmospheric pollutants, and the erosion of natural weather, wind, and rain, the painting of the West Gate shooting tower is seriously damaged (typical diseases of shooting tower painting are shown in Fig. 2). In many parts, the colored painting is faded and damaged, and dust and dirt are found on its surface, which seriously affects the long-term preservation of architectural painting.

In recent decades, with the rapid development of urbanization and the intensification of industrialization, the problem of air pollution has become an outstanding issue. Many harmful gases and particulate matter are discharged into the atmosphere, which causes corrosive damage to cultural heritage [3–7]. Therefore, it is necessary to fully investigate the main causes of damage and deterioration processes in cultural heritage to plan specific actions to prevent conservation. Many researchers investigated the relation between environmental pollution and the degradation phenomena on the built heritage, because of air pollution's rapid increase and growing harmfulness [8–13]. Among them, wet and dry deposition of sulfur dioxide (SO₂) and particulate matter (PM) in the air has been considered the main cause of deterioration of building materials in terms of soiling and blackening, which implied unaesthetic effects and chemical and physical consequences to the substrate. It is noteworthy that this decrease in SO₂ dates back to the 1970s, and this reduction is thanks to improvements to industrial plants and the use of low-sulfur fuels [14, 15]. On the contrary, emissions from vehicular traffic have

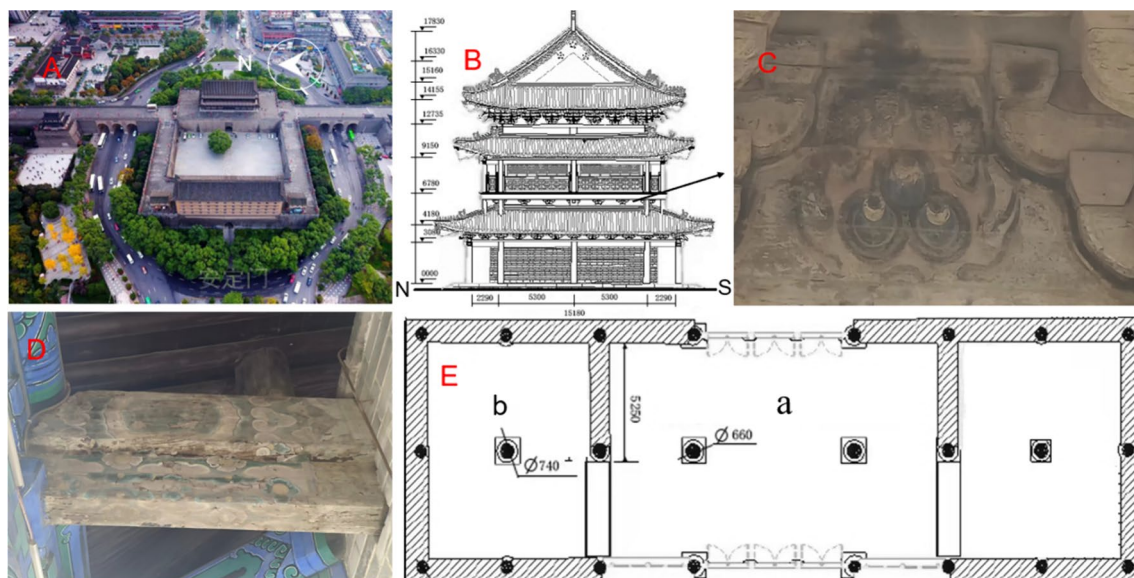


Fig. 1 Outline of sculptures of the archery tower at West Gate (A) aerial view of the archery tower; B north profile; C flame pearl patten; D the color painting of early Qing Dynasty and the Republic of China. E Schematic diagram of locations of monitoring points (a) located in the middle of the second floor of the archery tower; (b) located in the south of the second floor of the archery tower



Fig. 2 Typical diseases on color paintings of the archery tower at West Gate (a: overall preservation condition; b: local condition; c: faded; d: cracked; e: fallen off; f: covered by dust.)

recently become the main cause of pollution detected in the majority cities [16]. This increased vehicular use causes a greater release of pollutants into the atmosphere, some of which later accumulate on the surfaces and cracks of the historic buildings, thus accelerating the process of degradation of these buildings [17]. Air pollution has changed from the traditional coal-burning type to the composite pollution of the coal-burning type and motor vehicle exhaust. Deterioration is an irreversible and inevitable phenomenon that occurs at a rate and in a manner that depends on the environmental material type, the surrounding environment, and the chemical and physical processes involved. This change in emissions sources has possible consequences for the degradation of cultural heritage. Consequently, the identification of the main pollution sources has become essential to defining mitigation actions against the degradation and alteration phenomena of architectural color paintings.

Based on the above, we utilized the color painting of the archery tower at the West Gate as a case study to investigate the rapid deterioration mechanism of the color painting layer by air pollution. They were selected for historical-artistic relevance and location in an urban context characterized by different prevailing pollution sources. In this paper, through the investigation of the preservation environment of color paintings and simulation experiments, the influence of dust and environment on the color and condition of architectural paintings was

mainly studied. It aims to provide effective environmental management and preventive protection programs for architectural painting protection.

Sample collection and experimental analysis

(1) Temperature and humidity tests

The temperature and humidity of the second floor of the archery tower at West Gate were monitored for 3 months by the HE173 high precision temperature and humidity recording instrument, temperature precision: ± 0.5 °C, humidity accuracy: $\pm 3\%$ RH (Shenzhen Huatu Measurement and Control System Co., Ltd.)

(2) PM_{2.5} and PM₁₀ determination

A sampling point was selected in the middle of the bright room on the second floor of the inner eaves of the Xi'an Anding Gate. According to the Environmental Quality Status Report of Xi'an in the first quarter of 2018 released by the Ecological Environment Bureau of Xi'an in Shaanxi Province, China, the monthly average concentrations of particulate matter PM₁₀ and PM_{2.5} in Xi'an in the first quarter of 2018 were serious in January (Reference website: <https://view.officeapps.live.com>). So, in this research, the measurements in January were expected to represent the typically higher

winter concentrations, as an approximate “worst case” situation to be compared with guidelines. The sampling time was from January 21st to 22nd, 2019. The sampler was a HY-100ws medium flow sampler (Qingdao Hengyang Company), and the flow rate was set to 100 L/min³. Quartz filter membrane (ϕ 90 mm, Pall flex) was used; the sampling height was 1.5 m from the ground, and the filter membrane was kept at a constant temperature and humidity for 24 h before and after sampling. It was weighed with an analytical balance, and the subtraction of the weights before and after sampling is the sampling weight [18].

(3) ICP-MS analysis

A quarter of the sample filter was placed in a Teflon analysis tube, and 3 ml of distilled concentrated nitric acid and 1 ml of redistilled concentrated hydrochloric acid were added. Then put the analysis tube into the microwave digestion apparatus to digest for 48 min, and the digested solution was made up to 10 ml with deionized water, and the metal elements in the solution were analyzed by the ICP-MS model [19].

(4) IC analysis

Put 1/4 of the sample filter into a 10 ml test tube, add 5 ml of deionized water to completely submerge it, and after ultrasonic vibration for 20 min, the extracted solution is filtered with a 0.15 μ m microfiltration membrane. Repeat the above steps once, collect the filtrate twice, and combine them together for analysis using the Model 761 ion chromatograph of Met Rohm Company [20].

(5) XRD analysis

The collected dust was analyzed by Smart Lab, the manufacturer was Rigaku Corporation XRD analyzer for phase analysis, the tube voltage was 20–45 kV, the tube current was 10–200 mA, and the starting and ending angles were 5° and 60°, where the step angle is 0.01°.

(6) Preparation of color painting simulation samples

① Cut 8 wood blocks of 3×3 cm and divide them into two groups. ② Use a 400-mesh standard sifter to sieve the pigments of ultramarine, lime green, cinnabar, and red lead to obtain pigment powder; ③ Use gelatin with a concentration of 3% gelatin water to make a pigment paste of appropriate concentration, and then use a brush to evenly spread it on the surface of the upper wood block, with a thickness of about 0.1–0.2 mm, and wait for it to dry for later use. ④ Place one group on the

inside of the second floor of the archery tower and place, the other group outside the corridor on the second floor of the archery tower at West Gate. ⑤ The simulated samples were photographed regularly, and the dust on the surface was observed with an optical microscope.

(7) Chromaticity analysis

Color differences were obtained using the CIE L*a*b* color space model. Measurements were performed by a VS-450 spectrophotometer (X-Rite, USA) to measure the surface reflection spectrum curve and chromatic aberration changes of the color-painted layer for 7 days, 21 days, 42 days, and 100 days on two groups of color painting simulation samples placed in the archery tower at West Gate.

Results and discussion

Monitoring and evaluation results of the conservation environment of interior color painting

Temperature and relative humidity

Natural deterioration is the main cause of the damage to the matrix of a cultural relic's collections, and this damage is most closely related to the environment in which cultural relics are located [21–23]. From January to March 2019, the indoor temperature and humidity of the second floor of the archery tower at West Gate were continuously monitored. The two points were selected for this environmental monitoring, as shown in Fig. 1E. One is located in the middle of the second floor of the archery tower (Point a), and the other is located the south of the second floor of the archery tower (Point b). The variations of temperature and relative humidity (RH) at each monitoring point in the archery tower are shown in Fig. 3. During the monitoring period, the fluctuation of temperature and relative humidity (RH) at points a and b is almost identical, meaning that the temperature fluctuation changes little and the RH changes obviously. From Fig. 3a, it can be observed that the highest temperature was 14.2 °C, the maximum humidity was 71.3%, the minimum humidity was 21.2%, the average temperature was 6.7 °C, and the average humidity was 47.9%. From Fig. 4b, it can also be seen that the highest temperature was 13.3 °C, the maximum humidity was 66.3%, the minimum humidity was 22.9%, and the average humidity was 46.2%.

It is a well-established fact that various materials deteriorate differently when exposed to fluctuations in temperature and relative humidity. In order to safeguard valuable cultural relics from such detrimental effects, a variety of global standards have been devised for the storage and display environments of collections [24]. Conservation guidelines can differ significantly from one country to another, influenced by factors such as local

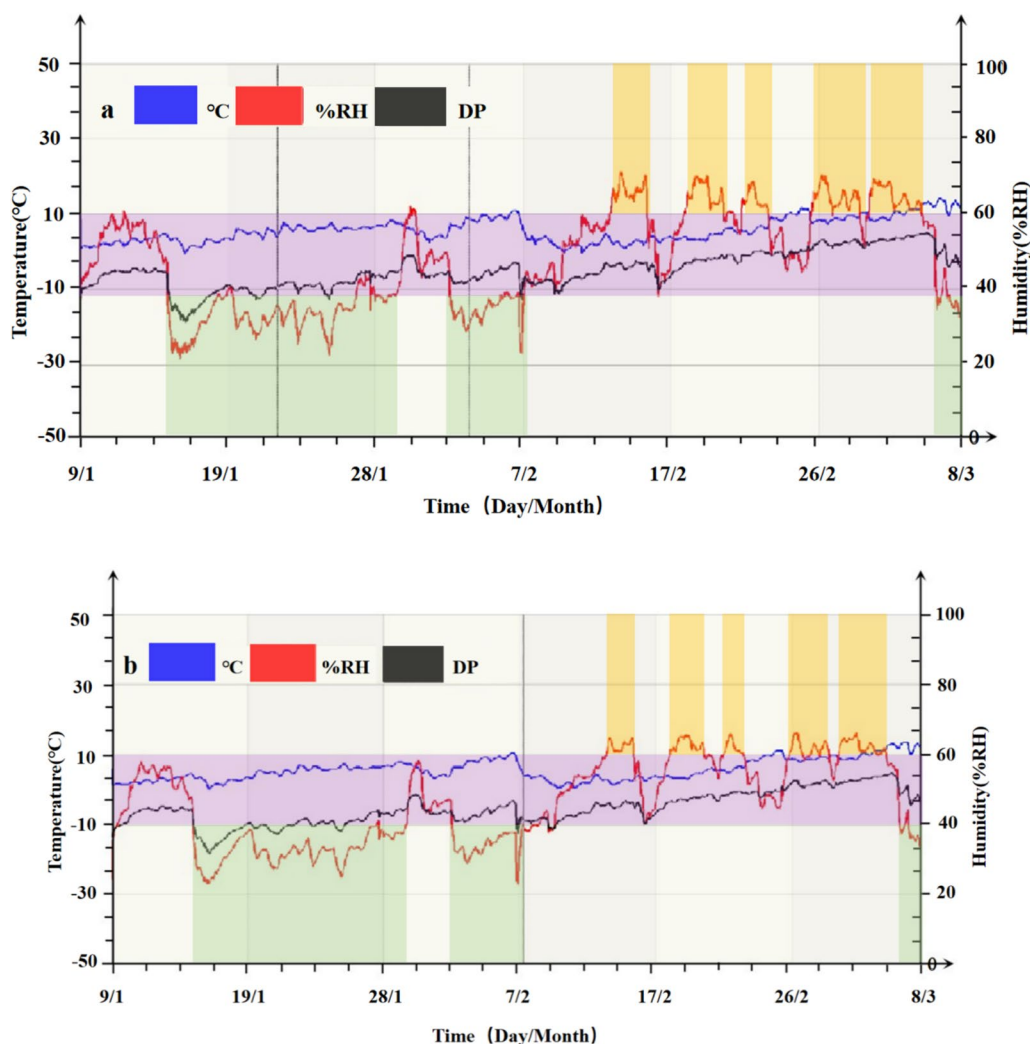


Fig.3 Temperature and relative humidity (%) of Point a and Point b during monitoring period

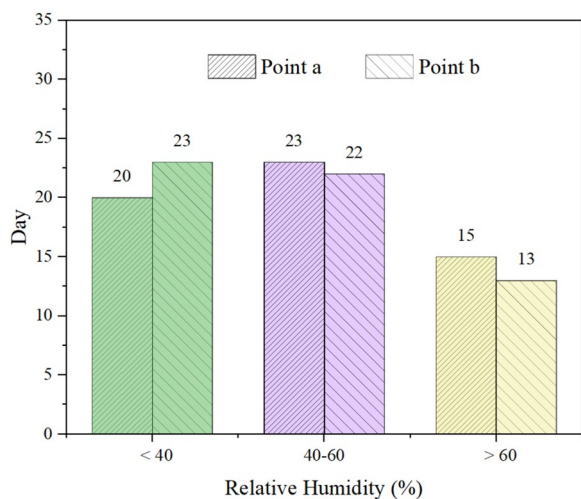


Fig.4 The days of different relative humidity range for Point a and Point b during monitoring period

climate conditions, collection types, and technological advancements. While specific temperature and humidity recommendations may vary regionally, the guidelines for wood-based materials tend to be the most consistent and least contentious. For optimal preservation of wood-based materials, a relative humidity level of 40–60% is considered ideal. Additionally, short-term humidity fluctuations within collection storage areas are typically limited to 5% or less [25]. The days of Point a and Point b in different relative humidity ranges were counted as shown in Fig. 4. The relative humidity of the middle of the second floor of the archery tower (point a) was lower than 40% in more than 34% of the days (about 20 days) during the monitoring period, with 26% of the days (about 15 days) having greater than 60%. Meanwhile, the RH fluctuations are obvious. there will cause the wood substrate to expand and contract, and the color layers to expand and contract unevenly, resulting in internal

stresses that could reduce their strength, which in turn could cause the colored painting layers to warp and fall off in a few years (see Fig. 2b, c). Therefore, the present environment is not conducive to the preservation of the color paintings of the archery tower at West Gate.

PM_{2.5} and PM₁₀ tests of the second floor of the archery tower

The concentration of pollutants in the conservation environment is an important factor in the long-term preservation quality of the architectural painting. PM is an important pollutant indicator to evaluate the quality of the storage environment. The aggressiveness of particles depends on their composition, size, hygroscopicity, and solubility. According to the National Environmental Quality Standards of the People’s Republic of China (GB 3095-2012, 2012), it is suggested that the A 24-h average PM_{2.5} and PM₁₀ concentrations in the preservation environment shall not exceed 75 µg/m³ and 150 µg/m³ [26, 27]. Table 1 shows the variation characteristics of PM_{2.5} and PM₁₀ average concentrations at the second floor of the archery tower during the monitoring period. It can

be seen from Table 1 that the A 24-h average PM_{2.5} in the air at the second floor of the archery tower at West Gate is 97.85 µg/m³ and 126.48 µg/m³, respectively. PM₁₀ was 264.65 µg/m³ and 301.46 µg/m³, which exceeded the level 2 nation standard (GB 3095-2012) by approximately 1.3–1.6 and 1.4–2.0. Evidently, the environmental conditions at the architectural painting of the archery tower fail to meet the necessary criteria for preservation. According to on-site investigation and research, the archery tower is not open to the public at present, no one cleans it, and the doors and windows are poorly sealed, which leads to dust entering the building and constantly deposited on the surface of the color painting. PM can cause the loss of hues, the loss of the density, and the change of color. Further damage can be caused when particles are moistened, a factor that makes them easier to react with other chemical compounds (SO₂ and NO_x) or with other materials with which they come into contact.

To determine the origin of these pollutants, we utilized ICP-MS to analyze the PM. The results (see Fig. 5) indicated that PM mainly contains inorganic elements Si, Ca, Al, Fe, K, Na, Mg, Cu, Zn, Pb, Cd, Ti, etc. Among them are Si > Ca > Al > Fe > K > Na > Mg. Si, Al, Fe, and Ca were the dominant chemical compositions of road dust of which Pb, and Zn elements mainly come from motor vehicle exhaust, brake pads and tire wear [28, 29]. We can see from Fig. 1a that the archery tower at West Gate is in the middle of the main road, surrounded by roads, where contamination through vehicular emissions is relatively high. While the weather conditions and high heating emissions in the cold season in northern China are

Table 1 Dust indoor monitoring results of color painting of the archery tower at West Gate (ug/m³)

Testing item	2019.01.21	2019.01.22
	Concentration	Concentration
PM _{2.5}	97	264
PM ₁₀	126	301
TSP	135	315

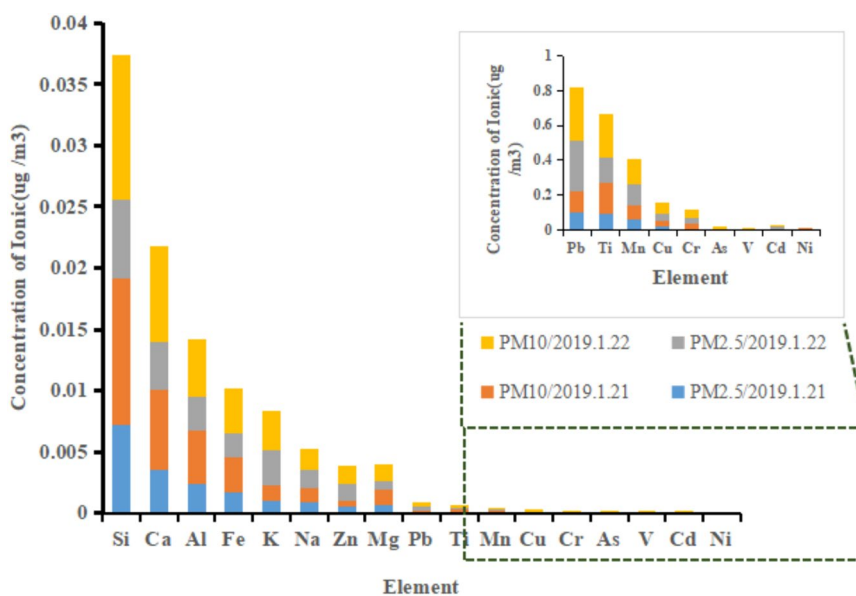


Fig. 5 Analysis results of indoor dust by ICP-MS (ug/m³)

conductive to dust emissions. Coal combustion is also a major contributor to Pb in the atmosphere. So, we think this dust is mainly from road dust and heating emissions [30, 31].

To investigate the potential impact of PM on color painting preservation, PM samples were subjected to X-ray diffraction analysis. The XRD results are shown in Fig. 6a. The X-ray diagrams of the dust adsorbed on the surface of the color painting show the presence of

quartz, gypsum, calcite, dolomite, plagioclase, chlorite, and illite. The content of gypsum, dolomite, calcite, and plagioclase in the dust is relatively high. Under a certain humidity, these compounds are deposited on the surface of architectural painting, which is easy to react with SO₂ and NO_x emitted by heating emissions or automobile exhaust gas after a series of reactions to generate SO₄²⁻ and NO₃⁻ in the form of soluble salt [32–35]. For example, the interaction between the

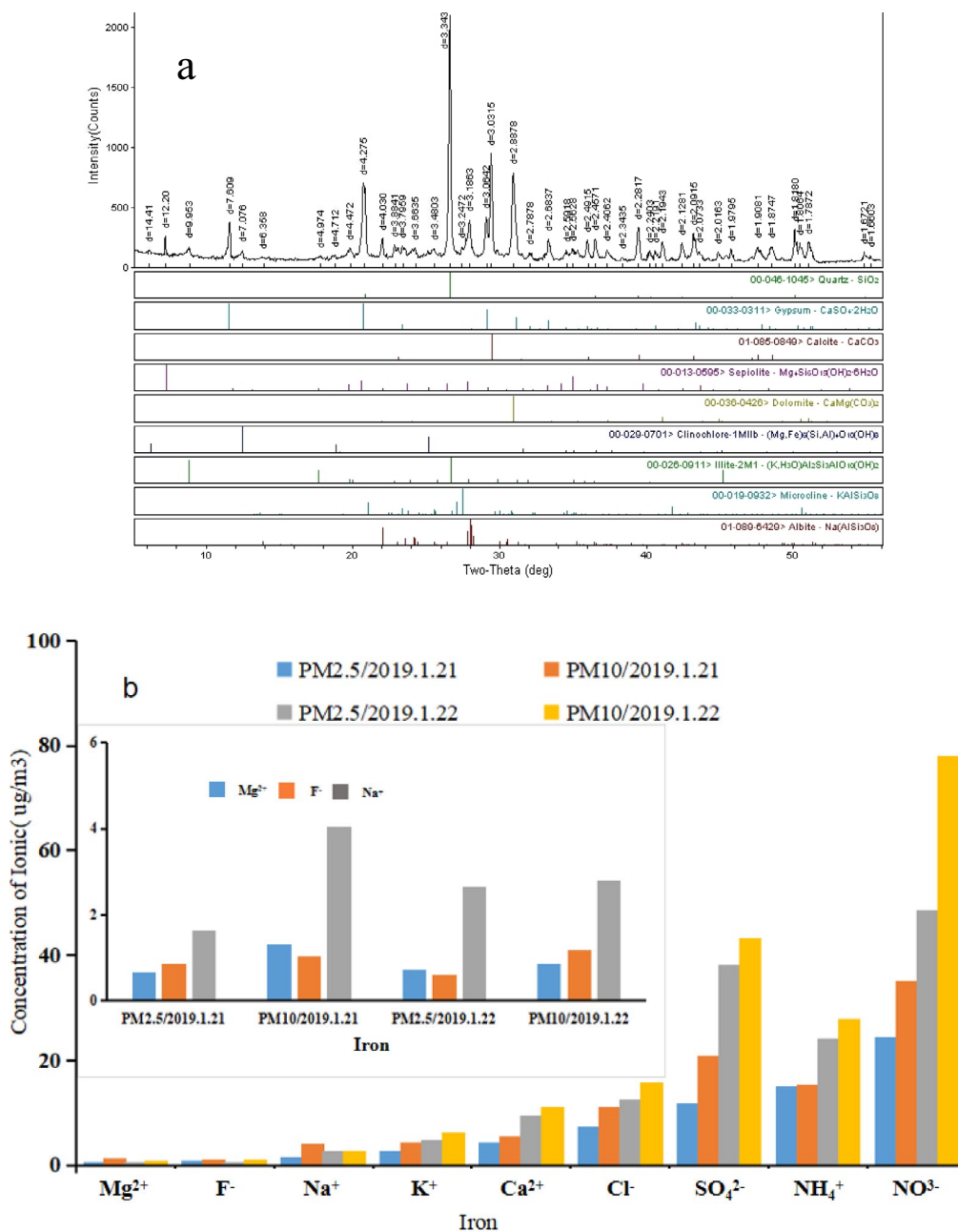
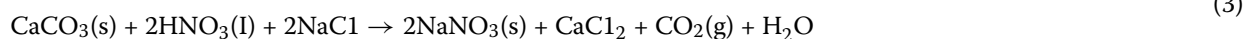
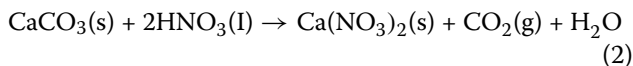


Fig. 6 The XRD (a) and IC (b) Results of indoor Dust Analysis

carbonate surface and the atmospheric aerosols is given by reactions (1)–(3) [36].



Due to the high solubility of the compounds formed, they can migrate through the pores of the color painting to the inner layers, corroding the painting.

The ion chromatography analysis in this work also yielded similar results. The IC findings (Fig. 6b) indicated the presence of calcium, potassium, sodium, magnesium, chloride, sulfate, and nitrate ions in these pollution samples. Among these, anions in dust are mainly composed of sulfate and nitrate due to their high rates.

The presence of soluble salts is a crucial factor contributing to the deterioration of color paintings. They can produce hydration, dehydration, and migration, yielding disintegration as well as the formation of florescences (e.g., gypsum, dehydrated, and hemihydrated casulfates). In a humid environment, this soluble salt promotes a volume or size change in the salt crystallized in their pores, which can be responsible for crack formations and fissures in the architectural painting [37]. In addition, nitrate salts (for instance, NaNO_3) are very hygroscopic salts with a high deposition rate [38]. Some studies have reported corrosion rates and deposition velocities of HNO_3 on calcareous stones and under low RH [39]. Therefore, the damage of soluble harmful ions in the dust of the above-mentioned air pollutants to the architectural painting could not be ignored. Dust particles and acidic

compounds accumulate over the color painting surfaces for a long time, which later causes slow and steady corrosion (Fig. 7).

Simulation experiment

Among the various hazards mentioned above, color change is also a problem because the architectural paint-

ing of the archery tower is losing its original hue, fading, becoming blurred, or darkening. According to the investigation results of the above PM survey, we conducted simulation experiments to elucidate the mechanism of PM's influence on the color of painting.

a) Visual observation of dust on the appearance and color of color painting simulation samples

Figure 8 is a visual photograph of the color change of the dust deposition on the surface of the painted simulation sample. The results show that the color painting surface of the four pigment swatches placed outdoors, with the extension of time, on the 42nd day, was covered with a lot of dust, and the apparent color had changed significantly. By the 100th day, the color of the painted surface had become dull and tarnished. Compared with the simulated samples of color paintings placed outdoors, the effect of dust on the apparent color of the color paintings is smaller. When the color of the four pigment swatches reaches 100 days, the color changes are relatively large, which also shows that indoor color paintings are less affected by dust than outdoor ones.

Through on-site investigation, at present, the dust on the surface of the color painting on the archery tower at West Gate mainly enters the room through the leaks in the doors and windows, and no one has cleaned it for a

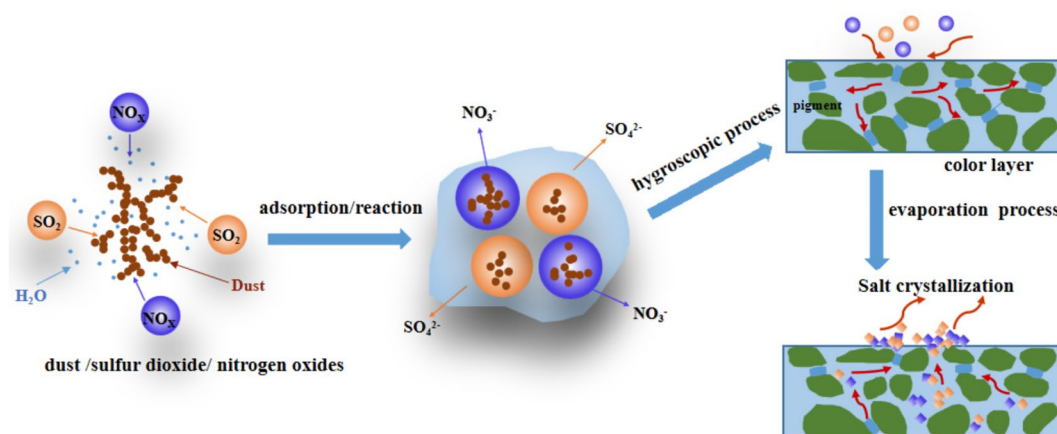


Fig. 7 The damage mechanism of PM on the color layer of architectural painting

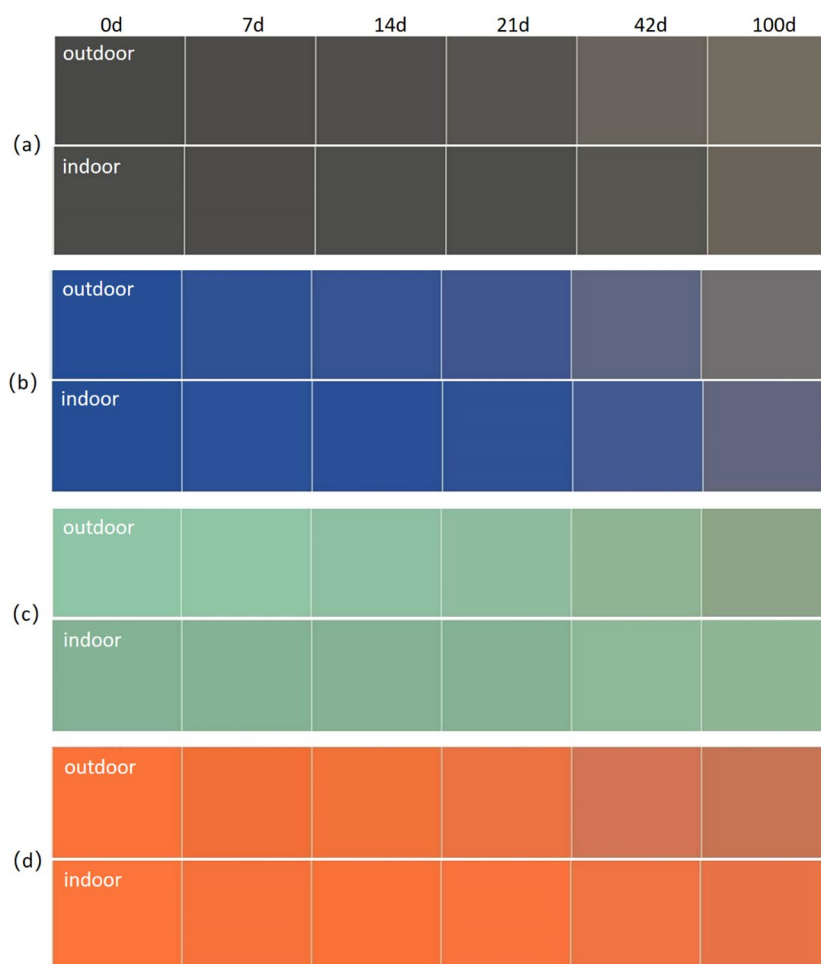


Fig. 8 Color appearance of dust deposition on the surface of the simulated sample in the color painting (a: carbon black; b: ultramarine blue; c: green; d: red lead)

long time. It is recommended to clean the indoor dust regularly in the later stage and improve the airtightness of the doors and windows, which will slow down or prevent the dust from entering the room.

b) Color reflection spectrum curve of color painting simulation samples

This study collected samples for indoor and outdoor experiments from January to March of 2019. Reflectance spectra and dust deposition amount data of color painting simulation samples were measured. Spectrometer was 350–2500 nm. The resolution was 3 nm, or 10 nm, and the sample interval was 1.37 nm, or 2 nm. The scanning interval of the spectrometer was 0.1 s. The spectral reflectance of the sample was obtained by averaging 10 original spectra of the same sample.

Figure 9 is the color reflection spectrum curve of the dust deposited on the surface of color painting simulation samples. In the visible light spectrum, the human

eye perceives color as having a red wavelength at 770–622 nm; an orange wavelength at 622–597 nm; a yellow wavelength at 597–577 nm; a green wavelength at 577–492 nm, and a blue wavelength at 492–455 nm. As can be seen from Fig. 9, the reflection spectrum of ultramarine blue pigment has the strongest absorption peak at 450 nm (Fig. 7b), stone green has the strongest absorption peak at 550 nm (Fig. 7c), and red lead has the strongest absorption peak at 620 nm (Fig. 7d), and carbon black fully absorbs at 350 nm–750 nm (Fig. 7a). Whether indoors or outdoors, the four pigments of the color painting simulation sample did not change the position of the reflection peak with the deposition of dust, the reflectance at the main peak position decreased, and the reflectance in other wavelength ranges increased, indicating that the adhesion of the dusty pigment introduces stray light of other wavelengths, which superimposes the main light and causes color distortion. It is further explained that the dust contaminates the color

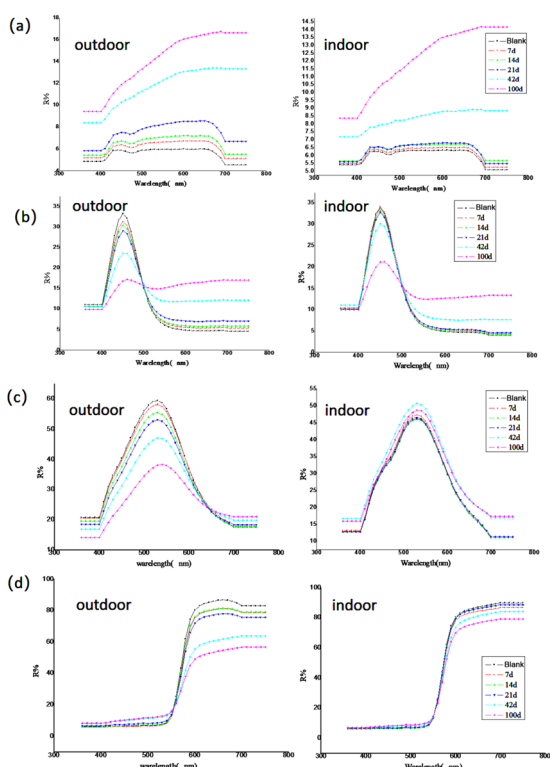


Fig. 9 Color reflection spectrum curve of the deposited dust on the surface of color painting simulation samples (a: carbon black, b: ultramarine blue, c: malachite green, d: red lead)

painting, which makes the color painting lose its original color. The color of opaque objects depends on the wavelength of the reflected light in the visible spectrum. Differences in the particle size and the crystal structure of dust can change the spectral reflectance of each band in the visible spectrum, thus changing the color appearance [40]. At the same time, once the dust settles and embeds in the micro-holes of the color painting, it covers

the color painting and makes its surface gray and black, which affects the aesthetic value and visual effect of the color painting. At the same time, compared with the change in reflectivity of indoor color painting simulation samples, with the prolongation of dust deposition time on the painted surface, the reflection curve of outdoor color painting simulation samples changes significantly. This situation is consistent with the conclusion of the color appearance diagram of color painting simulation samples.

Figure 10 is a micrograph of the painted layer of the indoor and outdoor painting simulation samples placed for 100 days. From the observations and the analysis of the data, the surface of the painted layer has a high density of dust particles, which can slow down the flux intensity of light and change the path of light. We think that when light strikes the color layer surface, one part of the light undergoes Fresnel reflection at the surface, the other part is refracted and enters the color layer, and the other part is absorbed. Noteworthy, we show only part of the rays escaping back into the air (Fig. 11). The incident light is only reflected on the surface of the color layer, as shown in Path 1. Or, as shown in Path 2, the incident light is refracted into the color layer and is eventually scattered. Going into details, because the pigment particles have colors, we see the color of the pigment particles after reflection and scattering; that is, the human eye receives the color. When dust is deposited

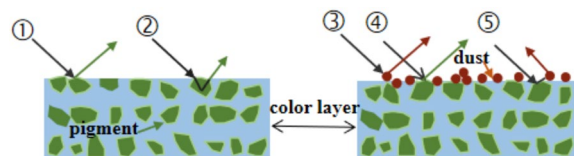


Fig. 11 Optical properties of surface color layers of simulation samples change before (a) and after (b) deposition of dust

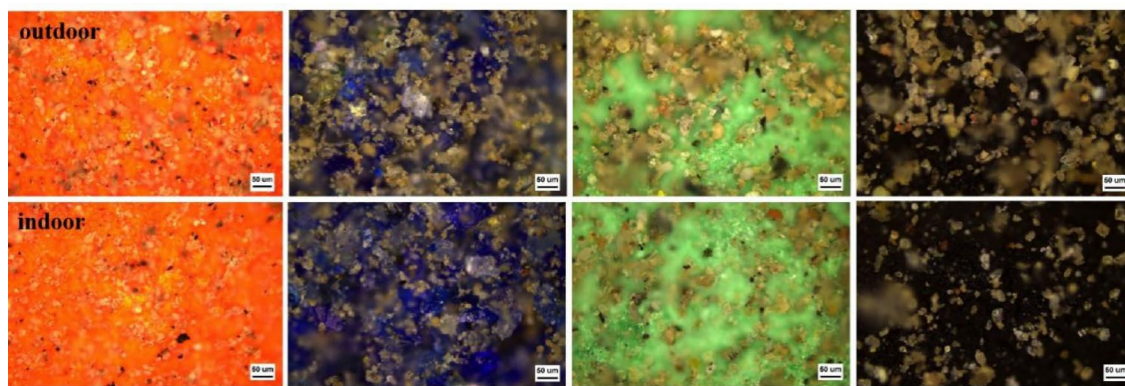


Fig. 10 The photomicrograph of dust deposition after 100 days on the surface of a painted simulated sample (x 20)

on the color lay surface as shown in Fig. 11b, due to the cover of dust, some light rays strike on the dust particles first, such as Path 3. A few light rays fall on the pigment particles, which are reflected as Path 4. Other light rays penetrate the pigment particles and are refracted, then scattered by the dust particles before reemerging as Path 5. Some wavelengths will decay during this process. As a result, the outgoing light will be reduced, and because the dust particles are colored, they are introduced, which eventually leads to a change in color.

c) chromaticity analysis of color painting simulation samples

In order to investigate the evolution of the color changes of the color painting simulation samples during the dust deposition, the space CIE L^*C^*h was applied [41]. In the space CIE L^*C^*h , the coordinate L^* represents the lightness, which varies from 0 (absolute black) to 100 (absolute white), and the C^* represents the purity of color and is explained by a vector from the center of the coordinate system to the place on the circle periphery determined by the hue angle. Hue (h) specifies the shades of the samples so that red, yellow, green, and blue colors are defined at 0, 90, 180, and 270°, respectively. The color difference was assessed based on ΔE^* as a measure of test accuracy. C^* , h^* , and ΔE^* are calculated as [42, 43]:

$$C_{ab}^* = \sqrt{a^{*2} + b^{*2}} \quad (4)$$

$$h_{ab}^* = \arctg\left(\frac{b^*}{a^*}\right) \quad (5)$$

$$\Delta E_{ab}^* = \sqrt{(\Delta L^*)^2 + (\Delta a^*)^2 + (\Delta b^*)^2} \quad (6)$$

$$\Delta L^* = L_x^* - L_0^* \quad (7)$$

$$\Delta a^* = a_x^* - a_0^* \quad (8)$$

$$\Delta b^* = b_x^* - b_0^* \quad (9)$$

where ΔE^* was the total color difference between milled and standard samples; ΔL^* , Δa^* , and Δb^* were the differences in luminance, red/green, and yellow/blue, respectively, between the milled and standard samples.

The variation in brightness (L^*), color intensity (C^*), hue (h), and overall color difference (E^*) of the diverse color painting simulation samples with the deposition of dust, are shown in Fig. 12. Notably, the analysis of color parameters revealed marked distinctions in the behavior of four specific pigments. It can be observed that the

variation of the L^* of carbon black and ultramarine blue increased gradually both outdoors and indoors throughout the test (as shown in Fig. 12a-1, b-1). Conversely, the L^* of red lead in indoor and outdoor decreased gradually with the test time, indicating that the red lead was gradually darkened by the deposition of dust (Fig. 12d-1). However, during the deposition of dust, the L^* value of malachite green showed an atypical behavior. The L^* value of the malachite green in indoor showed an increase trend, whereas outdoor showed a decrease (Fig. 12c-1).

The variations in the C^* of ultramarine blue, malachite green and red lead show that they are consistent. It is observed that C^* is obviously reduced with the extension of time, and the decrease outdoors is more obvious than that indoors (Fig. 12b-2, c-2, d-2). However, the variation C^* of carbon black obviously increases during the deposition of dust (Fig. 12a-2). For the variation h , the four color painting simulation samples in indoors and outdoors is decreasing (Fig. 12a-3, d-3, c-3 and d-3).

Differences in the behavior of the variations of L^* , C^* , and h were not statistically significant. However, the global color change ΔE^* is significant and pronounced for four color painting simulation samples (Fig. 12a-d), and it can be observed that the four pigments suffered, in the 100 days of the indoor/outdoor test, an intense increase. Meanwhile, the outdoor area is more affected by dust than the indoor area, indicating that with the increase in dust on the surface of the color painting, the original color of the color painting has been distorted. These findings confirmed the visual photographs of the color change result (Fig. 8).

Conclusion

In this study, by monitoring the preservation environment of the architectural painting of the archery tower at West Gate and conducting simulation experiments, the risk of architectural painting surface deterioration was assessed. The current research provides an important scientific basis for the preventive protection of the architectural painting of the archery tower at West Gate. The main conclusions are as follows:

- (1) The temperature and relative humidity (RH) in the color painting preservation environment were monitored for 3 months, and the results indicated that the indoor humidity fluctuated significantly during the monitoring period and most of the time exceeded the environmental standard requirements for the preservation of wooden cultural relics, which was not conducive to the preservation of color paintings, resulting in cracks, warping, and

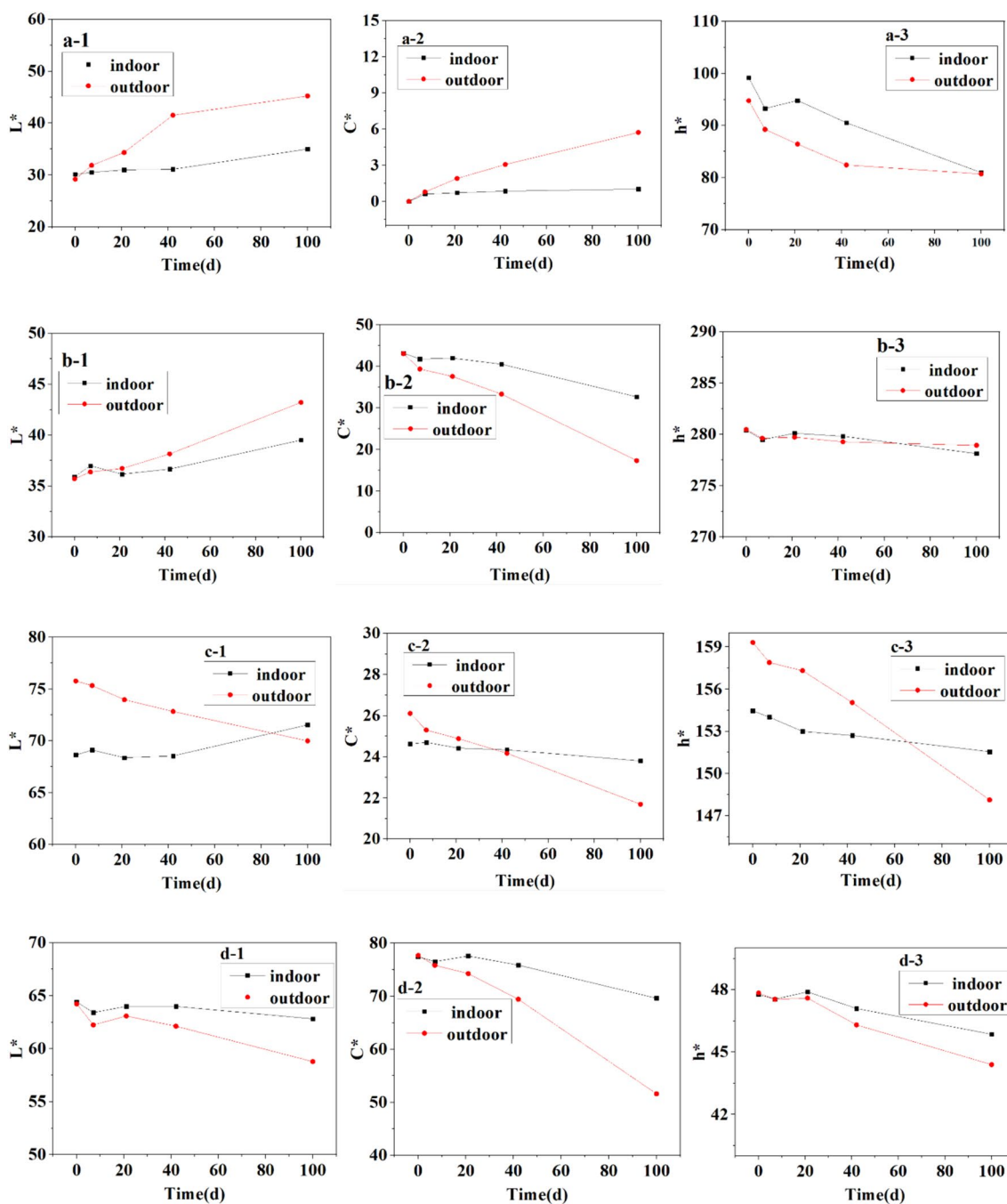


Fig. 12 The chromaticity value of dust deposited on the surface changes. (a: carbon black, b: ultramarine blue, c: malachite green, d: red lead)

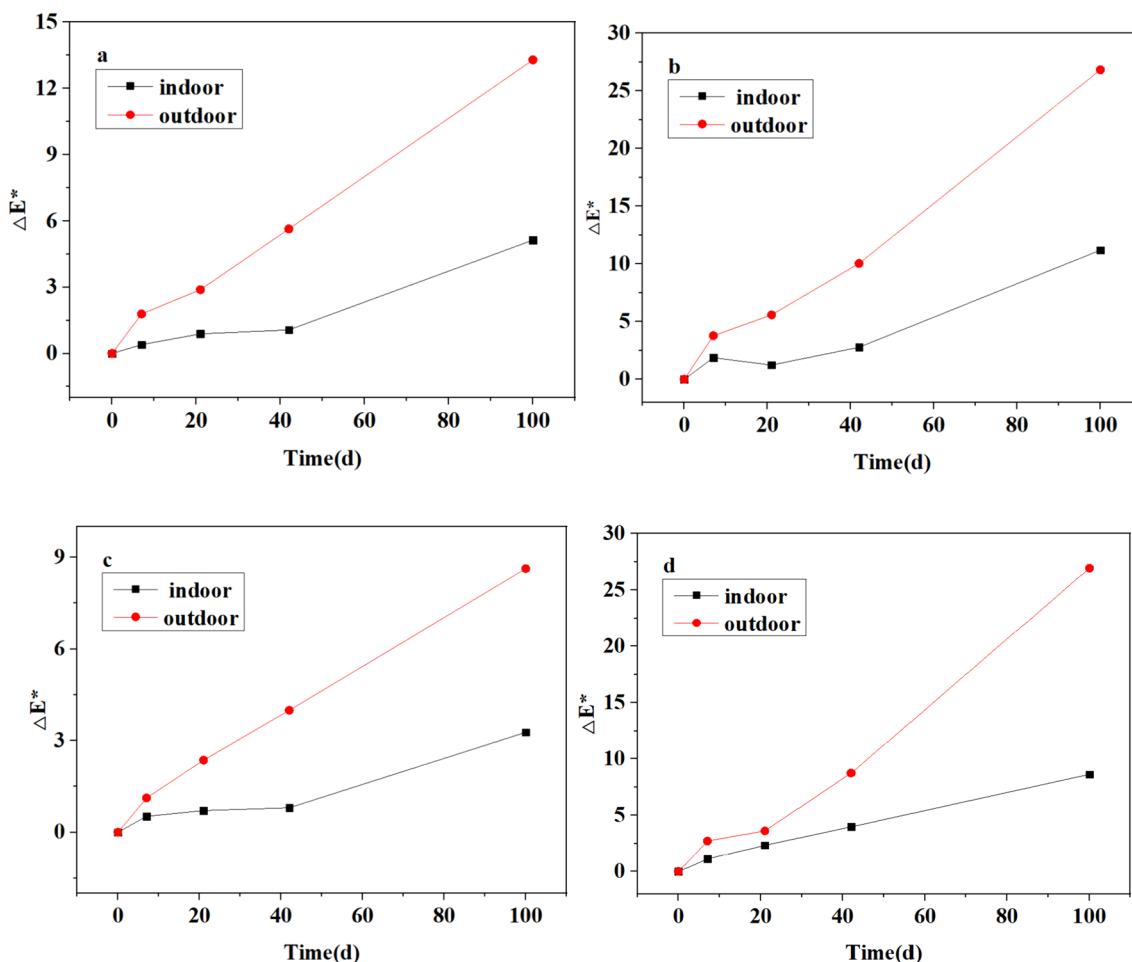


Fig. 12 continued

other diseases of color paintings, and the sealing of doors and windows should be strengthened.

- (2) Due to the poor sealing of the door and window of the tower, a large amount of dust is deposited on the surface of the color painting. These dust particles adsorb SO_2 and NO_x in the air in a humid environment, converting the dust particles into soluble nitrate and sulfate and aggravated the hygroscopic property of the color painting surface. Meanwhile, the risk of damage by water and salt had increased, thus resulting in chalking, peeling, and even falling off.
- (3) Through the simulation experiment of color painting, chromaticity analysis was carried out using the L^*C^*h color space model to analyze the influence of dust on color painting. The experimental results showed that the dust particles introduced stray light of other wavelengths, superimposed the main light, and caused color distortion in color painting.

Meanwhile, the results show that L^* values (luminance) decreased with increasing dust particles on the color painting surface as the color became progressively darker. ΔE^* showed an increasing trend, while h decreased with the increasing deposition time of dust particles. Further explaining the dust deposition on the surface of the color painting, resulting in the color losing its original hue, fading, becoming blurred, or becoming dark.

Hence, it is proposed that regular monitoring and analysis of major air pollutants in the vicinity of the archery tower at West Gate can provide background information to systematically ascertain their sources, pathways, and impacts, which are to be supplemented with the proper planning and management of regular maintenance and operations of the color painting of the archery tower at West Gate.

Author contributions

J. L. W. conceived the research, designed the research methodology, performed experiments, data acquisition and processing, and drafted the manuscript. P. F. and M. C. performed the data acquisition, W.Q.D and M. C. discussed the results and reviewed and corrected the manuscript. M. C., P. F. and W.Q.D have contributed equally to this work.

Funding

The authors gratefully acknowledge the financial support by the National Natural Science Foundation of China (No. 22372131), the Fundamental Research Funds for the Central Universities (GK 202103061 and GK 202103058), the Key Research and Development Program of Shaanxi Province, China (No. 2021SF-457). And the Key Research and Development Program of Xianyang City of Shaanxi Province, China (No. L2023-ZDYF-SF-003).

Data availability

The datasets used and/or analysis results obtained in the current study are available from the corresponding author on request.

Declarations

Competing interests

The authors declare that they have no conflicts of interest related to this work. We declare that we do not have any commercial or associative interest that represents a competing interests in connection with the work submitted.

Received: 10 April 2024 Accepted: 22 July 2024

Published online: 14 August 2024

References

- Su F. The shape and evolution of City wall and City Gate (Chengmen-dong) in Xi'an in Ming Dynasty. Xi'an University of Architecture and Technology, 2006.
- He L. Xi'an City Wall change gate tower maintenance project. *Cult Relics*. 2005;04:26–7.
- Chan C, Yao X. Air pollution in mega cities in China. *Atmos Environ*. 2008;42(1):1–42. <https://doi.org/10.1016/j.atmosenv.2007.09.003>.
- Gallego-Cartagena E, Morillas H, Maguregui M, Patino-Camelo K, Marcáida I, Morgado-Gamero W, Silva LFO, Madariaga JM. A comprehensive study of biofilms growing on the built heritage of a Caribbean industrial city in correlation with construction materials. *Int Biodeterior Biodegrad*. 2020;147:104874. <https://doi.org/10.1016/j.ibiod.2019.104874>.
- Oliveira MLS, Flores EMM, Dotto GL, Neckel A, Silvab LFO. Nanomineralogy of mortars and ceramics from the forum of Caesar and Nerva (Rome, Italy): the protagonist of black crusts produced on historic buildings. *J Clean Prod*. 2021;278:123982. <https://doi.org/10.1016/j.jclepro.2020.123982>.
- Ramírez O, da Boit K, Blanco E, Silva LFO. Hazardous thoracic and ultrafine particles from road dust in a caribbean industrial city. *Urban Clim*. 2020;33:100655. <https://doi.org/10.1016/j.uclim.2020.100655>.
- Saini A, Harner T, Chinnadhurai S, Schuster JK, Yates A, Sweetman A, Aristizabal-Zuluaga BH, Jim'enez B, Manzano CA, Gaga EO. GAPSmegacities: a new global platform for investigating persistent organic pollutants and chemicals of emerging concern in urban air. *Environ Pollut*. 2020;267:115416. <https://doi.org/10.1016/j.envpol.2020.115416>.
- Oliveira MLS, Neckel A, Pinto D, Maculan LS, Dotto GL, Silva LFO. The impact of air pollutants on the degradation of two historic buildings in Bordeaux France. *Urban Clim*. 2021;39:100927. <https://doi.org/10.1016/j.uclim.2021.100927>.
- Sesana E, Gagnon AS, Ciantelli C, Cassar JA, Hughes JJ. Climate change impacts on cultural heritage: a literature review. *WIREs Clim Change*. 2021;12(12): e710. <https://doi.org/10.1002/wcc.710>.
- Esteban-Cantillo OJ, Menendez B, Quesada B. Climate change and air pollution impacts on cultural heritage building materials in Europe and Mexico. *Sci Total Environ*. 2024;921:170945. <https://doi.org/10.1016/j.scitotenv.2024.170945>.
- Rovella N, Aly N, Comite V, Randazzo L, Fermo P, Barca D, Alvarez de Buergo M, La Russa MF. The environmental impact of air pollution on the built heritage of historic Cairo (Egypt). *Sci Total Environ*. 2021;764:142905. <https://doi.org/10.1016/j.scitotenv.2020.142905>.
- Comite V, Miani A, Ricca M, La Russa M, Pulimeno M, Fermo P. The impact of atmospheric pollution on outdoor cultural heritage: an analytic methodology for the characterization of the carbonaceous fraction in black crusts present on stone surfaces. *Environ Res*. 2021;201:111565. <https://doi.org/10.1016/j.envres.2021.111565>.
- Kontozova-Deutsch V, Cardell C, Urosevic M, Ruiz-Agudo E, Deutsch F, Van Grieken R. Characterization of indoor and outdoor atmospheric pollutants impacting architectural monuments: the case of San Jerónimo Monastery (Granada, Spain). *Environ Earth Sci*. 2010;63:1433–45. <https://doi.org/10.1007/s12665-010-0657-5>.
- Vidović K, Hočevnar S, Menart E, Drvenčić I, Grgić I, Kroflič A. Impact of air pollution on outdoor cultural heritage objects and decoding the role of particulate matter: a critical review. *Environ Sci Pollut Res*. 2022;29:46405–37. <https://doi.org/10.1007/s11356-022-20309-8>.
- Natarajan N, Vasudevan M, Dineshkumar SK, Nandhini SS, Balaganesh P. Effects of air pollution on monumental buildings in India: an overview. *Environ Sci Pollut Res*. 2021;29:29399–408. <https://doi.org/10.1007/s11356-021-14044-9>.
- Vidorni G, Sardella A, De Nuntiis P, Volpi F, Dinoi A, Contini D, Comite V, Vaccaro C, Fermo P, Bonazza A. Air pollution impact on carbonate building stones in Italian urban sites. *Eur Phys J Plus*. 2019;134:439. <https://doi.org/10.1140/epjp/i2019-12943-0>.
- Silva LFO, Oliveira MLS, Neckel A, Maculan LS, Milanés CB, Bodah BW, Cambruzzi LP, Dotto GL. Effects of atmospheric pollutants on human health and deterioration of medieval historical architecture (North Africa, Tunisia). *Urban Clim*. 2022;41:101046. <https://doi.org/10.1016/j.uclim.2021.101046>.
- Bailey AS, Jamieson HE, Radkova AB. Geochemical characterization of dust from arsenic-bearing tailings, giant mine. *Canada Appl Geochem*. 2021;135:105119. <https://doi.org/10.1016/j.japgeochem.2021.105119>.
- Camilleri R, Stark C, Vella AJ, Harrison RM, Aquilina NJ. Validation of an optimised microwave-assisted acid digestion method for trace and ultra-trace elements in indoor PM2.5 by ICP-MS analysis. *Heliyon*. 2023;9:e12844. <https://doi.org/10.1016/j.heliyon.2023.e12844>.
- Ozga I, Bonazza A, Bernardi E, Tittarelli F, Favoni O, Ghedini N, Morselli L, Sabbioni C. Diagnosis of surface damage induced by air pollution on 20th-century concrete buildings. *Atmos Environ*. 2011;45:4986–95. <https://doi.org/10.1016/j.atmosenv.2011.05.072>.
- Nastou MP, Zerefos S. Impacts of climate change on cultural heritage; the case of the greek theatre of dionysus. *Earth Environ Sci*. 2021;899:012020. <https://doi.org/10.1088/1755-1315/899/1/012020>.
- Zorpas AA, Skouroupatis A. Indoor air quality evaluation of two museums in a subtropical climate conditions. *Sustain Cities Soc*. 2016;20:52–60. <https://doi.org/10.1016/j.scs.2015.10.020>.
- Samadelli M, Zink AR, Roselli G, Gabrielli S, Tabandeh S, Ferricola VC. Development of passive controlled atmosphere display cases for the conservation of cultural assets. *J Cult Herit*. 2019;35:145–53. <https://doi.org/10.1016/j.culher.2018.05.005>.
- Guo C, Lan L, Liu Y, Meng N, Li C. Comparison of environmental criteria for conservation and storage of collections: a comprehensive literature review. *Build Environ*. 2023;243:110665. <https://doi.org/10.1016/j.buildenv.2023.110665>.
- GJ 66–2015, Code for Design of Museum Buildings, Ministry of Housing and Urban-Rural Construction of the People's Republic of China, 2015.
- GB 3095–2012, Ambient Air Quality Standards, Ministry of Environmental Protection of the People's Republic of China, 2012.
- Chen P, Bi X, Zhang J, Wu J, Feng Y. Assessment of heavy metal pollution characteristics and human health risk of exposure to ambient PM2.5 in Tianjin China. *Particuology*. 2015;20:104–9. <https://doi.org/10.1016/j.partic.2014.04.020>.
- Shen Z, Sun J, Cao J, Zhang L, Zhang Q, Lei Y, Gao J, Huang R, Liu S, Huang Y, Zhu C, Xu H, Zheng C, Liu P, Xue Z. Chemical profiles of urban fugitive dust PM2.5 samples in Northern Chinese cities. *Sci Total Environ*. 2016;569–570:619–26. <https://doi.org/10.1016/j.scitotenv.2016.06.156>.
- Sun J, Shen Z, Zhang L, Lei Y, Gong X, Zhang Q, Zhang T, Xu H, Cui S, Wang Q, Cao J, Tao J, Zhang N, Zhang R. Chemical source profiles of urban fugitive dust PM2.5 samples from 21 cities across China. *Sci Total*

- Environ. 2018;649:1045–53. <https://doi.org/10.1016/j.scitotenv.2018.08.374>.
30. Lin Z, Ji Y, Lin Y, et al. PM10 and PM2.5 chemical source profiles of road dust over China: composition, spatio-temporal distribution, and source apportionment. *Urban Clim.* 2023;51:101672. <https://doi.org/10.1016/j.uclim.2023.101672>.
 31. Jayarathne A, Egodawatta P, Ayoko G, Goonetilleke A. Geochemical phase and particle size relationships of metals in urban road dust. *Environ Pollut.* 2017;230:218–26. <https://doi.org/10.1016/j.envpol.2017.06.059>.
 32. Yun J, Zhu C, Wang Q, Hu Q, Yang G. Catalytic conversions of atmospheric sulfur dioxide and formation of acid rain over mineral dusts: molecular oxygen as the oxygen source. *Chemosphere.* 2019;217:18–25. <https://doi.org/10.1016/j.chemosphere.2018.10.201>.
 33. Wang T, Liu Y, Deng Y, Fu H, Zhang L, Chen J. Adsorption of SO₂ on mineral dust particles influenced by atmospheric moisture. *Atmos Environ.* 2018;191:153–61. <https://doi.org/10.1016/j.atmosenv.2018.08.008>.
 34. Olson E, Michalski G, Welp L, Larrea Valdivia AE, Reyes Larico J, Salcedo Peña J, Fang H, Magara Gomez K, Li J. Mineral dust and fossil fuel combustion dominate sources of aerosol sulfate in urban Peru identified by sulfur stable isotopes and water-soluble ions. *Atmos Environ.* 2021;260:118482. <https://doi.org/10.1016/j.atmosenv.2021.118482>.
 35. Spezzano P. Mapping the susceptibility of UNESCO World cultural heritage sites in Europe to ambient (outdoor) air pollution. *Sci Total Environ.* 2021;754:142345. <https://doi.org/10.1016/j.scitotenv.2020.142345>.
 36. Martínez-Arkarazo I, Angulo M, Bartolomé L, Etxebarria N, Olazabal MA, Madariaga JM. An integrated analytical approach to diagnose the conservation state of building materials of a palace house in the metropolitan Bilbao (Basque Country, North of Spain). *Anal Chim Acta.* 2007;584:350–9. <https://doi.org/10.1016/j.aca.2006.11.046>.
 37. Gulzar S, Burg J-P. Preliminary investigation of late Mughal period wall paintings from historic monuments of Begumpura Lahore. *Front Archit Res.* 2018;7:465–72. <https://doi.org/10.1016/j.foar.2018.08.001>.
 38. Zhang H, Gu W, Li YJ, Tang M. Hygroscopic properties of sodium and potassium salts as related to saline mineral dusts and sea salt aerosols. *J Environ Sci.* 2020;95:65–72. <https://doi.org/10.1016/j.jes.2020.03.046>.
 39. Vidal F, Vicente R, Mendes SJ. Review of environmental and air pollution impacts on built heritage: 10 questions on corrosion and soiling effects for urban intervention. *J Cult Herit.* 2019;37:273–95. <https://doi.org/10.1016/j.culher.2018.11.006>.
 40. Liu M, Peng Z, Wang X, He Y, Huang S, Wan J, Wang B, Zhou Y, Yang H, Zheng H. The effect of high energy ball milling on the structure and properties of two greenish mineral pigments. *Dyes Pigm.* 2021;193:109494. <https://doi.org/10.1016/j.dyepig.2021.109494>.
 41. Sheikh N, Babrud RB, Khatamifar F. The effect of gamma irradiation to eliminate fungal contamination on two model colors of Iranian paintings. *Radiat Phys Chem.* 2021;189:109704. <https://doi.org/10.1016/j.radphyschem.2021.109704>.
 42. Hatami L, Jamshidi M. Effects of type and duration of pigment milling on mechanical and colorimetric properties of colored self compacting mortars (CSCM). *J Build Eng.* 2021;35:102006. <https://doi.org/10.1016/j.jobbe.2020.102006>.
 43. Rivas T, Pozo-Antonio JS, Barral D, Martínez J, Cardell C. Statistical analysis of colour changes in tempera paints mock-ups exposed to urban and marine environment. *Measurement.* 2018;118:298–310. <https://doi.org/10.1016/j.measurement.2017.06.037>.

Publisher's Note

Springer Nature remains neutral with regard to jurisdictional claims in published maps and institutional affiliations.